The equilibrative nucleoside transporter ENT1 is critical for nucleotide homeostasis and optimal erythropoiesis

Mahmoud Mikdar, Pedro González-Menéndez, Xiaoli Cai, Yujin Zhang, Marion Serra, Abdoul Dembele, Anne-Claire Boschat, Sylvia Sanquer, Cerina Chhuon, Ida Chiara Guerrera, et al.

The equilibrative nucleoside transporter 1 (ENT1) is critical for nucleotide homeostasis and optimal erythropoiesis

Mahmoud Mikdar[1,2,3], Pedro González-Menéndez[†3,4], Xiaoli Cai[†,5], Yujin Zhang[5], Marion Serra[1,2,3], Abdoul K Dembele[1,2,3], Anne-Claire Boschat[6], Sylvia Sanquer[7], Cerina Chhuon[8], Ida Chiara Guerrera[8], Marc Sitbon[4], Olivier Hermine[3,9], Yves Colin[1,2,3], Caroline Le Van Kim[1,2,3], Sandrina Kinet[3,4,*], Narla Mohandas[10,*], Yang Xia[5,*,#], Thierry Peyrard[1,2,3,**,#], Naomi Taylor[3,4,11,* *,#], Slim Azouzi[1,2,3,**,#]

[1]Université de Paris, UMR_S1134, BIGR, Inserm, F-75015 Paris, France.

[2]Institut National de la Transfusion Sanguine, F-75015 Paris, France.

[3]Laboratoire d'Excellence GR-Ex, Paris, France.

[4]Institut de Génétique Moléculaire de Montpellier, Univ Montpellier, CNRS, Montpellier, France.

[5]Department of Biochemistry and Molecular Biology, University of Texas McGovern Medical School at Houston.

[6]Plateforme de spectrométrie de masse, Imagine Institute, Paris, France.

[7]Inserm UMR-S 1124, Université de Paris, Service de Biochimie Métabolomique et Protéomique, Hôpital Necker Enfants malades, Assistance Publique-Hôpitaux de Paris, Paris, France.

[8]Université de Paris, Proteomics Platform 3P5-Necker, Structure Fédérative de Recherche Necker, Inserm US24/CNRS, UMS3633, Paris, France

[9]Université de Paris, UMR 8147, CNRS, 75014-Paris, France

[10]New York Blood Center, New York, NY, USA

[11]Pediatric Oncology Branch, NCI, CCR, NIH, Bethesda, MD, USA

[#]To whom correspondence should be addressed:

- Slim Azouzi, Inserm, UMR_S1134, INTS, 6 rue Alexandre Cabanel, 75015 Paris, France; E-mail: slim.azouzi@inserm.fr; Phone: +33144493041; Fax: +33143065019.
- Naomi Taylor, Pediatric Oncology Branch, NCI, CCR, NIH, Bethesda, MD, USA; Email: taylorn4@mail.nih.gov.
- Thierry Peyrard, Inserm, UMR_S1134, INTS, 6 rue Alexandre Cabanel, 75015 Paris, France; E-mail: tpeyrard@ints.fr; Phone: +33155251204; Fax: +33143065019.
- Yang Xia, Department of Biochemistry and Molecular Biology, University of Texas McGovern Medical School at Houston; Email: yang.xia@uth.tmc.edu; Phone: 713-500-5039; Fax: 713-500-0652.

[†,*,**] Equal contribution

Short title: Role of ENT1 in murine and human erythropoiesis

Key points:

- Deficiency of the equilibrative nucleotide transporter ENT1 results in abnormal erythropoiesis in humans and mice
- Inhibition of the ABCC4 cyclic nucleotide exporter enhances erythroid differentiation in the absence of ENT1.

Text word count: 4248

Number of figures: 6

Number of references: 73

Supplemental file: Methods; 16 supplemental figures; 3 supplemental Tables.

Supplemental Excel file: comparative phosphoproteomic analysis

Abstract

The tight regulation of intracellular nucleotides is critical for the self-renewal and lineage specification of hematopoietic stem cells (HSCs). Nucleosides are major metabolite precursors for nucleotide biosynthesis and their availability in HSCs is dependent on their transport through specific membrane transporters. However, the role of nucleoside transporters in the differentiation of HSCs to the erythroid lineage and in red cell biology remains to be fully defined. Here, we show that the absence of the equilibrative nucleoside transporter (ENT1) in human red blood cells (RBCs) with a rare Augustine-null blood type (AUG:-1) is associated with macrocytosis, anisopoikilocytosis, an abnormal nucleotide metabolome, and deregulated protein phosphorylation. A specific role for ENT1 in human erythropoiesis was demonstrated by a defective erythropoiesis of human $CD34^+$ progenitors following shRNA-mediated knockdown of ENT1. Furthermore, genetic deletion of ENT1 in mice was associated with reduced erythroid progenitors in the bone marrow, anemia and macrocytosis. Mechanistically, we found that ENT1-mediated adenosine transport is critical for cAMP homeostasis and the regulation of erythroid transcription factors. Notably, genetic investigation of two $ENT1_{null}$ individuals demonstrated a compensation by a loss-of-function variant in the *ABCC4* cyclic nucleotide exporter. Indeed, pharmacological inhibition of ABCC4 in $Ent1^{-/-}$ mice rescued erythropoiesis. Overall, our results highlight the importance of ENT1-mediated nucleotide metabolism in erythropoiesis.

Introduction

The commitment of hematopoietic stem cells (HSCs) to the erythroid lineage is a complex process controlled by extrinsic factors as well as the physical interaction of HSCs with their microenvironment[1–5]. Nutrient resources and their transport has recently emerged as key regulators of HSC proliferation and lineage commitment[6–8]. Notably, a sufficient intracellular nucleotide pool has been shown to be essential for erythroid lineage commitment of HSCs[6]. Nucleotide biosynthesis is regulated by the intracellular availability of glutamine and the shunting of glucose from glycolysis pathway through the pentose phosphate pathway[6]. Nucleotides are indispensable precursors for RNA and DNA synthesis and are extremely important for cell division[9,10]. Balanced pools of intracellular nucleotides are crucial to avoid DNA damage in erythroid and lymphoid lineages[11–14]. Furthermore, nucleotide homeostasis is also crucial for terminal erythroid differentiation and the generation of mature red blood cells (RBCs). cAMP- and cGMP-mediated signaling is associated with the regulation of erythropoiesis through the modulation of numerous signaling pathways[15–23] and the activation of important erythroid-specific transcription factors[24,25].

HSCs lack the capacity to carry out *de novo* nucleoside synthesis[26] and thus rely on membrane transporters to acquire nucleosides for DNA and RNA synthesis and ATP production[26]. The major source of nucleoside recycling is the degradation of nucleic acids, arising from autophagic (or phagocytic) pathways[26] and the degradation of nucleotides in the extracellular compartment. The equilibrative nucleoside transporter 3 (ENT3) is the major nucleoside transporter responsible for maintaining nucleoside homeostasis in lysosomal and mitochondrial compartments[27,28]. In humans, ENT3 alteration causes numerous genetic disorders with a wide spectrum of clinical manifestations including hematological abnormalities[29–33]. Mechanistically, the altered commitment of ENT3-deficient HSCs is caused by the loss of

lysosomal adenosine transport, which impedes autophagy-regulated HSC fates[33]. However, ENT1 is the major plasma membrane transporter in HSCs that ensures nucleoside uptake from the extracellular compartment[34,35]. ENT1 plays a central role in the homeostasis of plasma adenosine which is generated extracellularly by the degradation of ATP *via* the ectonucleotidases CD39 and CD73[36,37]. While extracellular uptake of nucleosides is an important step in nucleotide biosynthesis, its specific contribution in driving HSC lineage commitment remains to be defined. This is of critical interest as humans with ENT1 deficiency, due to a c.589+1G>C mutation in the *SLC29A1* gene encoding ENT1, have recently been described[38].

Here, we demonstrate that ENT1 deficiency in humans and mice is associated with erythroid defects and identify a functional link between ENT1 and ABCC4-mediated cyclic nucleotide metabolism in erythroid differentiation. Our genetic and pharmacological findings open new avenues for the development of novel therapeutic strategies for the treatment of anemia.

Methods

Detailed protocols for all methods are provided in supplemental methods.

Blood samples

Fresh peripheral blood samples were obtained from healthy donors from the Etablissement Français du Sang (EFS) and $ENT1_{null}$ patients after obtaining written informed consent.

Ex vivo erythropoiesis

Human primary CD34 cells, isolated from the peripheral blood of patients and healthy donors or from cord blood, were cultured as described in the Supplemental Methods.

Lentiviral ENT1 knockdown

ENT1 was downregulated in $CD34^+$ progenitors using an shRNA approach.

Metabolomics and phosphoproteomics

Phosphoproteomic analyses were performed using the label free proteomic methodology. Intracellular pools of nucleotides were quantified by high-performance liquid chromatography mass spectrometry (HPLC-MS).

***Ent1*$^{-/-}$ mice model**

All protocols involving animal studies were reviewed and approved by the Institutional Animal Welfare Committee of the University of Texas Health Science Center at Houston.

Results

ENT1-deficiency in human RBCs is associated with membrane and metabolomic disorders

A homozygous splicing mutation in the *SLC29A1* gene was previously identified in three Augustine-null phenotype siblings (P1, P2, P3), resulting in total deficiency of ENT1[38] (Figure 1A; Supplemental Figure S1). RBC indices of the three ENT1$_{null}$ probands revealed macrocytosis (MCV; 104-108 fL) and increased cell hemoglobin (Hb) content (MCH; 34-37 pg) but normal cell Hb concentration (MCHC) (Supplemental Table S1). The normal reticulocyte counts in all probands are consistent with the absence of anemia and hemolysis (normal LDH and haptoglobin values). However, morphological examination revealed >40% of RBCs with altered cell shapes and sizes, a characteristic of anisopoikilocytosis, in all three patients (Figure 1B). While RBCs from P1 and P2 showed similar morphological alterations, the blood smear of P3 revealed a more severe phenotype with the presence of elliptocytes and a higher percentage of schizocytes (Figures 1B; 1C). Furthermore, in conjunction with more severe morphological abnormalities, RBC membrane deformability was impaired in the P3 proband as reflected by the extent of increase in Elongation Index (EI) as a function of increasing applied shear stress[39] (Figure 1D). ENT1$_{null}$ RBCs displayed heterogenous osmotic gradient ektacytometry profiles, confirming distinct RBC changes in these patients with the profile in P3 consistent with elliptocytosis (Figure 1E). This macrocytosis was not due to

deficiency of either Vitamin B12 or folate in $ENT1_{null}$ probands since their levels were within the normal range (539±134 pmol/L and 9.2±0.2 nmol/L, respectively). Except for moderate ectopic mineralization also observed in *slc29a1*$^{-/-}$ mice[40], $ENT1_{null}$ probands did not exhibit significant non-hematological clinical manifestations[38].

To further evaluate the RBC membrane defect in $ENT1_{null}$ RBCs, we performed a comparative global phosphoproteomic analysis of RBC membrane proteins. This analysis was performed as changes in cyclic nucleotide levels have long been known to impact protein kinases and thereby the phosphorylation state of the cell[41]. Phosphoproteome analysis identified 501 serine, threonine and tyrosine phosphorylation sites in 182 cytoskeletal and transmembrane proteins across all samples (Supplemental Excel file). Ten serine sites were differentially hypophosphorylated in eight proteins from $ENT1_{null}$ RBCs (Figure 1F, $p<0.01$; Supplemental Figure S2); these proteins included membrane proteins such as spectrin, ankyrin, adducin and protein 4.1 as well as non-membrane proteins such as ALDOA. Notably, these membrane proteins form a complex that is critical for membrane stability and RBC morphology[42,43]. Interestingly though, Triton X-100 extractability of these proteins from $ENT1_{null}$ RBCs was unchanged compared to controls (Supplemental Figure S3), suggesting that other molecular mechanism(s) besides spectrin-based skeletal complexes underlie the abnormal RBC morphology of $ENT1_{null}$ individuals. On the other hand, two proteins were hyperphosphorylated in $ENT1_{null}$ RBCs as compared to controls; the chloride nucleotide-sensitive channel CLNSA1 (also called pICln) and PNPLA6 (Figure 1F, $p<0.01$). Interestingly, CLNSA1 has been shown to regulate RBC volume *via* its interaction with the 4.1R protein[44]. Moreover, some differences in protein phosphorylation can be appreciated among $ENT1_{null}$ ghosts (Supplemental Excel file).

As ENT1 is the major nucleoside transporter in RBCs[45], we evaluated the nucleotide-derived metabolites in ENT1$_{null}$ RBCs by HPLC-MS. Importantly, we noted that the intracellular levels of both purine and pyrimidine nucleotides (dCTP, dCDP, CMP, GTP, and dATP) were significantly increased in ENT1$_{null}$ RBCs compared to control RBCs (Figure 1G, $p<0.05$, $p<0.01$ and $p<0.001$). This accumulation of deoxynucleotides (dNTPs) in ENT1$_{null}$ RBCs could either be due to the altered dNTP uptake from the plasma, or to an inappropriate uptake of dNTPs by the mitochondria of ENT1$_{null}$ erythroblasts since ENT1 has been implicated in dNTP transport across the mitochondrial membrane[46–48]. Concerning the cyclic nucleotides, there were no statistically significant differences in cAMP levels between patient and control RBCs (Figure 1G). Interestingly though, cGMP levels were extremely variable, with high levels in RBCs from P1 and P2 and very low levels in P3.

These data indicated that the absence of ENT1 results in a greater phenotypic change in red cells from patient P3 as compared to patients P1 and P2. We therefore performed whole exome sequencing (WES) to assess whether other genetic variant(s) might account for these differences (Figure 1H). Analyzing WES data by filtering common pathogenic variants shared by P1 and P2, and not P3, led to the identification of a heterozygous loss-of-function variant in *ABCC4* gene (c.559 G>T; p.Gly187Trp). *ABCC4* encodes a cyclic nucleotide exporter highly expressed in erythroid precursors (Figure 1I)[49]. Interestingly, this finding is consistent with the 6.3- and 5.2-fold higher level of cGMP in P1 and P2 RBCs, respectively, as compared to controls (Figure 1G). Moreover, cGMP levels in P3 RBCs were actually 2.8-fold lower than in control RBCs. Thus, the *ABCC4* mutation in P1 and P2 is associated with a significant increase in RBC cGMP levels as compared to P3 and healthy controls, and may function to compensate for the loss of ENT1.

Differences in the *ex vivo* erythroid differentiation potential of CD34$^+$ progenitors from ENT1$_{null}$ individuals

Having documented alterations in mature erythrocytes from $ENT1_{null}$ individuals, we investigated the role of ENT1 during erythropoiesis. *Ex vivo* erythropoiesis of $CD34^+$ cells from the peripherical blood of all three $ENT1_{null}$ patients was investigated. $CD34^+$ progenitors from P1 and P2 underwent erythroid differentiation in the presence of rEPO with increased expression of the GPA and Band 3 erythroid markers, to similar levels as control progenitors (Figure 2A). Furthermore, *in vitro* reticulocyte levels for both patients at day 12 were similar to controls (40±2% *vs* 38±6% in two independent experiments, respectively), indicating that the absence of ENT1 in erythroid precursors from P1 and P2 did not inhibit erythroblast enucleation (Figure 2B). Interestingly, macrocytic reticulocytes were observed from the *ex vivo* erythroid culture of P2 (Supplemental Figure S4).

In contrast to P1 and P2, $CD34^+$ progenitors from P3 patient failed to undergo *ex vivo* erythroid differentiation (n=4; Figure 2A). Only 16±5% of P3 cells acquired GPA expression at day 5 as compared to 88±9% for controls (Figure 2A and Figure 2C, $p<0.0001$). Furthermore, within the GPA^+ subset, only 3±2% erythroblasts exhibited an up regulation of Band3 *versus* 24±6% in control erythroblasts (Figure 2C, $p<0.001$). This markedly delayed erythroid differentiation was associated with increased cell death (Figure S5) and markedly decreased cell proliferation (Figure 2D, $p<0.01$). The ineffective *in vitro* erythropoiesis of P3 progenitors was confirmed by MGG staining, revealing immature erythroblasts in controls conditions while myeloid cells were noted in cultures of P3 patient (Figure 2E). Furthermore, only 4% of P3 progenitors progressed to the erythroid colony forming unit (CFU-E) stage, defined as $IL3R^-CD34^-CD36^+$, as compared to 33% of control progenitors (Figure 2F). Consistent with these data, P3 $CD34^+$ cells failed to give rise to colony-forming unit-erythroid (CFU-E) colonies in methylcellulose assays while control cells were able to form large BFU-E and CFU-E colonies (Figure 2G). Interestingly, this defect may be due to alterations in the characteristics of $CD34^+$ progenitors migrating to the peripheral circulation; while $CD34^+$ cells generally account for approximately

0.5% of PBMC[50] and we detected 0.63% $CD34^+$ cells in a representative healthy donor, the percentage of $CD34^+$ progenitors in P3 was much lower, at 0.17% (Figure S6). Altogether, our findings highlight a difference in the ability of circulating $CD34^+$ progenitors from P1/P2, as compared to P3, to undergo *ex vivo* erythroid differentiation.

shRNA-mediated knockdown of ENT1 inhibits erythroid differentiation of $CD34^+$ progenitors

In order to specifically assess the impact of ENT1 on erythropoiesis, we pursued an shRNA-mediated ENT1-knockdown strategy as illustrated in Figure 3A. Monitoring the surface expression profile of ENT1 during erythropoiesis by flow cytometry showed a high-level expression of ENT1 on progenitor cells prior to rEPO stimulation (day 0) followed by a gradual decrease during terminal erythroid maturation (Figure 3B). Transduction of cord blood $CD34^+$ progenitors with an shENT1 lentiviral vector resulted in a pronounced reduction in *SLC29A1* mRNA levels (90±4%, Figure 3C) and a concomitant decrease in cell surface expression of ENT1 (40±8% at day 0, Supplemental Figures S7A; SB). While ENT1 knockdown did not significantly alter expression of CD34, CD36 or IL3R prior to rEPO-induced erythroid differentiation (day 7, Figure S8), shENT1-transduced progenitors were counter-selected following addition of EPO. The percentages of GFP^+ cells decreased by more than 50% between day 0 and day 5 of erythroid differentiation and by more than 80% at day 7 (Figure 3D). The negative impact of ENT1 knockdown was specific for erythroid differentiation as the percentage of shENT1-GFP^+ progenitors remained stable upon expansion of $CD34^+$ progenitors in the absence of rEPO (Figure 3D). In addition, the EPO-induced expansion of GFP^+ cells was significantly lower for shENT1-transduced as compared to shControl-transduced progenitors (Figure 3E). These findings strongly suggest that ENT1 expression is crucial for erythroid, but not non-erythroid, differentiation.

To address the effect of ENT1 down-regulation on terminal erythroid differentiation, we monitored the surface expression of the GPA and CD71 erythroid markers. EPO-induced erythroid differentiation of hematopoietic progenitors was significantly attenuated following ENT1 down-regulation, and notably, this effect was only detected in the shENT1-transduced subset (Figures 3F; 3G). At day 3 of differentiation, only 42±5% and 41±8% of shENT1-transduced cells expressed GPA and CD71, respectively, as compared to 55±9% and 66±5% of shControl-transduced cells ($p<0.01$ and $p<0.05$; Figure 3G). Consistent with this finding, erythroblast enucleation was significantly reduced in shENT1-GFP-transduced cells (5±2% *vs* 20±6%, $p<0.05$; Figure 3H). In addition, flow cytometry analysis revealed that >25% of shENT1-transduced progenitors expressed the CD11a and CD33 myeloid markers as compared to only 4% of control cells ($p<0.05$; Figure 3I). Overall, these findings reveal an important role for ENT1 in erythroid differentiation.

Ent1$^{-/-}$ mice resemble ENT1$_{null}$ patients displaying macrocytic RBCs and exhibit altered erythroid lineage differentiation

To assess whether the absence of ENT1 in humans results in similar alterations in ENT1$_{null}$ mice, we analyzed the complete blood count (CBC) in 8-12-week old *Ent1*$^{-/-}$ mice as compared to their wild-type counterparts. Both male and female *Ent1*$^{-/-}$ mice exhibited a macrocytosis and increased MCH that was similar to that detected in ENT1-deficient patients (Supplemental Table S2); blood smears revealed an increased size of RBCs in *Ent1*$^{-/-}$ mice (Figure 4A) as well as a significantly increased mean corpuscular volume (MCV) ($p<0.01$). Additionally, RBC numbers and hematocrit were reduced in both male and female *Ent1*$^{-/-}$ mice as compared with gender-matched control mice (Supplemental Table S2). These findings point to similarities as well as differences in the erythroid phenotype resulting from ENT1 deficiency in humans and mice.

Erythropoiesis is initiated from BM-derived HSCs that differentiate to common myeloid progenitors (CMPs), followed by commitment to megakaryocyte erythroid progenitors (MEPs) *vs* granulocyte myeloid progenitors (GMPs). MEPs generate erythroid progenitors that undergo terminal differentiation to generate mature RBCs[51,52] (Figure 4B). Given that *Ent1*$^{-/-}$ mice displayed mild anemia, we evaluated the phenotype of hematopoietic progenitors in their BM as compared to WT mice. There were no differences in the number of Lin^{-}cKit^{+} cells between both mice groups (Figure 4C). However, *Ent1*$^{-/-}$ mice displayed a significant decrease in CMP (CD34^{+}CD16/32^{-}) and MEP (CD34^{-}CD16/32^{-}) cells but an increased GMP (CD34^{+}CD16/32^{-}) cells compared to WT mice ($p<0.05$, Figure 4C). These data point to decreased erythroid differentiation and indeed, the percentage of Ter119^{+} erythroid cells in the BM of *Ent1*$^{-/-}$ mice was lower than WT mice, while the level of Gr-1^{+} granulocytes was increased ($p<0.05$, Figure 4D).

In mice, the spleen is the major site for stress erythropoiesis[53]. Surprisingly, we found that *Ent1*$^{-/-}$ mice displayed splenomegaly ($p<0.05$, Figure 4E) compared with their WT counterparts at 8-12-week age, raising an intriguing possibility of an increased erythropoiesis to counteract the anemic state of these mice. Interestingly, flow cytometry analysis of erythroid precursors in the spleen showed an increase in early progenitors (populations I and II) with equivalent levels of later progenitors (Figure 4F). Thus, there is an increase in the total splenic Ter119^{+} population in *Ent1*$^{-/-}$ mice (Figure 4G). To rule out the possibility that the splenomegaly in *Ent1*$^{-/-}$ mice is due to increased clearance of RBCs by the spleen, we measured red cell life span by labeling all circulating erythrocytes *in vivo* by injection of *N*-succinimidyl-6-[biotinamido] hexanoate. The percentage of biotinylated erythrocytes in the circulation in *Ent1*$^{-/-}$ mice was not decreased as compared to WT mice (Figure 4H), strongly suggesting that increased RBC destruction was not responsible for the splenomegaly detected in *Ent1*$^{-/-}$ mice.

ENT1-mediated adenosine uptake induces cyclic nucleotide accumulation and enhanced *in vitro* erythropoiesis

The abnormal protein phosphorylation and nucleotide metabolome in human mature $ENT1_{null}$ RBCs, in conjunction with the increased adenosine plasma levels in $ENT1_{null}$ probands ($p< 0.0001$, Supplemental Figure S9), as previously reported for *Ent1*$^{-/-}$ mice[54], confirm the importance of adenosine as a substrate of ENT1. In order to address the question of whether ENT1 regulates erythropoiesis *via* its capacity to transport adenosine, we performed *ex vivo* differentiation of $CD34^+$ progenitors from healthy donors following addition of adenosine. Enhanced terminal erythroid differentiation was noted in the presence of adenosine (15 μM), a concentration that did not alter proliferation or survival (not shown). Differentiation was monitored as a function of α4-integrin/ Band3 staining on GPA^+ cells, with an α4-integrin^{low}/ Band3^{low} phenotype representing the most differentiated erythroblasts. Notably, adenosine significantly accelerated erythroid differentiation in control progenitors (Figures 5A; 5B) and this finding was also confirmed by MGG staining (Figure 5C). However, adenosine did not enhance erythroid differentiation following shRNA-mediated knockdown of ENT1, as monitored by GPA and Band3 expression (Figures 5D; 5E), and did not rescue shENT1-transduced progenitors from being negatively selected (Figure S10). These data are in accord with ENT1's role as a major adenosine transporter expressed in erythroid precursors[34,35]. Furthermore, shENT1-transduced progenitors upregulated myeloid lineage markers despite the presence of rEPO and adenosine (Figure 5D). These findings demonstrate the inability of adenosine to enhance erythroid differentiation in the absence of ENT1, strongly suggesting that ENT1 regulates erythroid differentiation via its role as adenosine transporter.

Since adenosine is an important precursor in the synthesis of other adenine nucleotides, we analyzed the nucleotide metabolome of control erythroblasts cultured in the presence of adenosine. Interestingly, the cyclic nucleotides cAMP and cGMP were significantly increased

in erythroblasts treated with adenosine (Figure 5F). Phosphorylation of the cAMP-response element-binding (CREB) protein, a transcription factor activated by cyclic nucleotides, decreased as a function of erythroid differentiation (Supplemental Figure S11). However, under conditions where extracellular adenosine was increased, CREB phosphorylation was increased (Figure 5G and Supplemental Figure S12). Accordingly, PKA phosphorylation was also significantly increased in the presence of adenosine, confirming an adenosine-stimulated cyclic nucleotide biosynthesis (Figure 5H). Together, these data reveal the importance of ENT1 in mediating adenosine uptake to regulate cyclic nucleotide biosynthesis and erythropoiesis.

Role of ABCC4 in cyclic nucleotide homeostasis in ENT1$_{null}$ cells

While all ENT1$_{null}$ patients exhibited macrocytosis, the impact of ENT1 on RBC deformability was more pronounced in P3 as compared to P1/P2. Furthermore, *in vitro* erythroid differentiation was altered in P3 progenitors but was not significantly attenuated in P1 and P2 progenitors. The attenuated erythroid phenotype of P1 and P2 as compared to P3 was associated with increased RBC cyclic nucleotide levels (Figure 1G). In addition, P2 erythroblasts exhibited an increased accumulation of cAMP and cGMP as compared to control erythroblasts, while shENT1-transduced erythroblasts exhibited a reduced level of cAMP (Supplemental Figures S13 and S14). Thus, ENT1 may regulate erythropoiesis via cyclic nucleotide metabolism and our data further suggest that a mutation in *ABCC4* compensates for the absence of ENT1, attenuating the erythroid phenotype in patients P1 and P2.

To test this hypothesis, we evaluated the effect of an ABCC4 inhibitor (MK-571) on *ex vivo* erythropoiesis of healthy donors (Supplemental Figure S15A). As shown in Figure 6, MK-571 significantly enhanced erythropoiesis as indicated by the increased GPA expression (Figure 6A). Moreover, MK-571 increased terminal erythroblast maturation and dramatically increased enucleation by approximately 2-fold ($p<0.05$, Figure 6B; 6C). MK-571 also enlarged the pool

of erythroid cells as shown by a significant increase in expansion without changes in apoptosis or cell death (Supplemental Figures S15B; S15C).

To specifically evaluate the impact of ABCC4 function on erythroid differentiation in the murine system, we inhibited ABCC4 function in *Ent1*$^{-/-}$ mice with MK-571[55]. Retro-orbital administration of MK-571 (10mg/kg for 6 days) increased total RBCs, Hb and hematocrit in *Ent1*$^{-/-}$ mice to levels similar to those detected in WT mice (Figure 6D). Interestingly though, MK-571 treatment did not alter red cell macrocytosis in *Ent1*$^{-/-}$ mice, strongly suggesting that erythropoiesis, but not macrocytosis, is regulated by ABCC4 in the absence of ENT1. Moreover, our data suggest that ABCC4 negatively regulates erythroid differentiation even in the presence of ENT1. MK-571 treatment significantly increased total RBCs, Hb production and hematocrit in WT mice. MK-571 treatment increased the percentage of circulating reticulocytes in both *Ent1*$^{-/-}$ and WT mice (Figure 6D), supporting this newly described association between ABCC4 and ENT1 in erythropoiesis. We then evaluated the potential impact of this drug on early stages of erythroid commitment. MK-571 treatment led to an increased percentage of BM MEPs in both WT and *Ent1*$^{-/-}$ mice ($p<0.05$ and $p<0.001$, respectively; Figures 6E and Supplemental Figure S16), but did not alter the percentage of Lin^{-}/cKit^{+} progenitors in either group (Figure 6F). This increase was associated with a significantly decreased percentage of BM GMPs in WT mice as well as BM CMPs in *Ent1*$^{-/-}$ mice ($p<0.05$; Figures 6E). This MEP/CMP shift was coupled to a significant increase in BM Ter119^{+} erythroid cells in both WT and *Ent1*$^{-/-}$ mice and a decreased percentage of Gr-1^{+} cells in BM of WT mice (Figure 6G). These experiments, performed on patient cells and following pharmacological manipulation of both human and murine ENT1$^{-/-}$ progenitors, highlight a novel crosstalk between ABCC4 and ENT1 in regulating erythroid differentiation.

DISCUSSION

Here, we show that ENT1$_{null}$ RBCs exhibit a defective phosphorylation of membrane proteins that is associated with distinct misshaped cells, confirming the crucial role of ENT1-mediated nucleoside transport in the regulation of metabolic pathways and kinase activities. While the finely-tuned regulation of membrane protein phosphorylation has previously been shown to be critical in the control of cell volume and membrane organization *via* ion channel activities and protein-protein interactions, respectively[42,56–59], our finding of dNTPs accumulation in ENT1$_{null}$ RBCs, reveals an important role of ENT1 in deoxynucleotide recycling and nucleotide homeostasis during erythroid diffrentiation[48]. Balanced nucleotide pools, controlling replication stress, DNA damage, protein kinases, as well as transcription factors,[19,23,60–62] have been shown to regulate hematopoietic lineage fate[13,14]. Indeed, we provide unequivocal demonstration that ENT1-mediated adenosine transport regulates the intracellular level of cyclic nucleotides in hematopoietic progenitors, altering erythroid differentiation under conditions where the phosphoproteome of ENT1$_{null}$ RBCs is abnormal. Finally, our data shows that knockdown of ENT1 in human CD34^{+} progenitors impede *in vitro* erythropoiesis while increasing ENT1-mediated adenosine transport enhances erythroid differentiation.

The absence of anemia in ENT1$_{null}$ patients is particularly intriguing considering the numerous erythroid alterations including, macrocytosis, anisopoikilocytosis and abnormal deformability. These data are even more surprising given that *Ent1*$^{-/-}$ mice exhibit a reduced RBC count, Hb and hematocrit. Interestingly though, red cells in *Ent1*$^{-/-}$ mice are not destroyed and ENT1$_{null}$ patients exhibit normal hemolysis markers. These data suggest that the lifespan of murine and human ENT1$_{null}$ RBCs is not shortened (Supplemental Table S1). In this regard, it is notable that neither S-adenosyl-methionine nor nucleotides are significantly altered in mature murine *Ent1*$^{-/-}$ red cells[63]. An attractive hypothesis to explain differences in the role of Ent1 in murine *versus* human red cell differentiation may be related to the hypoxia-mediated up regulation of key metabolites, including nucleotides, within the low-oxygen BM microenvironment[54,64–66].

The hypoxic microenvironment of the BM niche influences the metabolic pathways used by HSCs and consequently their erythroid differentiation. In line with these findings, we have recently shown that ENT1 and adenosine signaling are involved in the adaptation to high-altitude hypoxia[45]. Thus, molecules and signaling networks that are yet to be identified may complement ENT1 function in the murine spleen where Ter119+ cells were increased as compared to bone marrow where erythroid differentiation was negatively impacted. Furthermore, while the specific ablation of Ent1 in erythroblasts, using an EpoR-Cre, also resulted in macrocytosis[67] , RBC numbers as well as other RBC parameters were less affected than those reported here using a complete Ent1 knockout. These data therefore raise the important possibility that ENT1 plays a role in erythroid differentiation at a progenitor stage upstream of $EpoR^+$ erythroblasts.

Our findings reveal a critical role of ABCC4 in regulating erythroid differentiation in the absence of ENT1 and moreover, we find that inhibition of ABCC4 enhances human and murine erythroid differentiation under physiological conditions. Notably, we identified ABCC4 as a crucial factor by documenting its role in explaining the differences in the *ex vivo* erythroid differentiation potential of P1 and P2 progenitors as compared to P3 progenitors. Mechanistically, we found that P1/P2 RBCs exhibited high levels of intracellular cyclic nucleotides whereas P3 RBCs are characterized by low cyclic nucleotide levels. This significant difference was associated with a heterozygous loss-of-function variant in the *ABCC4* cyclic nucleotide exporter in P1/P2, but not in P3. The finding that ABCC4 inhibitor significantly rescued the anemic phenotype and increased erythroid differentiation in *Ent1*$^{-/-}$ mice strongly suggests a crosstalk between ABCC4 and ENT1 in regulating erythropoiesis. Notably though, ABCC4 inhibition did not correct the macrocytic phenotype of these *Ent1*$^{-/-}$ mice, indicating that in our murine model, the macrocytic red cell phenotype is ABCC4-independent. Collectively, these data indicate that the intracellular level of cyclic nucleotides is crucial for *in*

vivo erythropoiesis and highlight the interdependence of the ABCC4 and ENT1 transporters in erythropoiesis.

In conclusion, we show that ENT1 plays a key role in nucleotide homeostasis and optimal erythropoiesis and provide both genetic and pharmacological evidence that ABCC4 is a key negative regulator of erythropoiesis in the absence of ENT1, exacerbating a perturbation in cyclic nucleotide homeostasis and downstream erythroid defects. Moreover, we find that inhibition of ABCC4 by MK-571 results in a rescue of the anemic phenotype in *Ent1*$^{-/-}$ mice, and an enhanced RBC production in WT mice without a significant reduction in circulating white blood cells. Notably, MK-571 has been tested in clinical trials as a therapeutic molecule to treat asthma[68–70], pulmonary arterial hypertension (PAH)[71], and platelet aggregation[55,72,73], *via* increasing the intracellular levels of cAMP and cGMP. The impact of MK-571 in PAH was specific to its effects on ABCC4 as deletion of this gene resulted in a notable reduction in hypoxia-induced inflammatory response[71]. MK-571 could therefore represent a novel drug for the therapeutic treatment of anemia.

Acknowledgments

We are indebted to Bérengère Koehl for helpful comments and for reading the manuscript. The authors are grateful to Cédric Vrignaud and Romain Duval for their assistance at CNRGS in this research project. We thank Sara El Hoss, Sandrine Laurence and Niloofar Reihani for their help with methylcellulose cultures. We also thank Martina Moras and Marie Daumur for their assistance. This work was supported by the Institut National de la Santé et de la Recherche Médicale (Inserm), the Institut National de la Transfusion Sanguine, and the Laboratory of Excellence GR-Ex, reference ANR-11-LABX-0051. The Labex GR-Ex is funded by the IdEx program “Investissements d’avenir” of the French National Research Agency, reference ANR-18-IDEX-0001. Mahmoud Mikdar was funded by the Ministère de l’Enseignement Supérieur et de la Recherche (Ecole Doctorale BioSPC); he also received financial support from the

Institut National de la Transfusion Sanguine. Pedro Gonzalez-Menendez was founded by the CLARIN-COFUND program from the Principado de Asturias and the European Union. This work is also supported by the FRM (to NT), National Institutes of Health PO1 DK032094 (to MN, SK and NT), HL137990 (to YX), HL136969 (to YX) and the McGovern Fund at the University of Texas Health Science Center-McGovern Medical School (YX).

Author Contributions

CLVK, YC, OH, MS, NT, TP, and SA conceived the project and obtained funding. MM, SK, NT, and SA designed the research study and YX oversaw the design of the *in vivo* mouse studies. TP collected human samples and clinical data of $ENT1_{null}$ patients. MM, PGM, and SK performed most of the experiments. XC conducted the *in vivo* mouse studies; ACB and SS realized the metabolomic analyses; CC and CG performed the phosphoproteomic studies; and YZ performed mouse blood smear experiments. MM, PGM, XC, MSe, AKD, SK, NM, TP, YX, NT, and SA analyzed the data. MM, NM, NT and SA wrote the manuscript with editing from PGM, SK, MS, XC, CLVK, TP, and YX.

Conflict of Interest Disclosures

The authors declare no conflict of interest.

REFERENCES

1. Oburoglu L, Romano M, Taylor N, Kinet S. Metabolic regulation of hematopoietic stem cell commitment and erythroid differentiation. *Curr. Opin. Hematol.* 2016;23(3):198–205.
2. An X, Mohandas N. Erythroblastic islands, terminal erythroid differentiation and reticulocyte maturation. *Int. J. Hematol.* 2011;93(2):139–143.
3. Rhodes MM, Kopsombut P, Bondurant MC, Price JO, Koury MJ. Adherence to macrophages in erythroblastic islands enhances erythroblast proliferation and increases

erythrocyte production by a different mechanism than erythropoietin. *Blood*. 2007;111(3):1700–1708.

4. Chasis JA, Mohandas N. Erythroblastic islands: niches for erythropoiesis. *Blood*. 2008;112(3):470–8.
5. BESSIS MC, BRETON-GORIUS J. Iron metabolism in the bone marrow as seen by electron microscopy: a critical review. *Blood*. 1962;19(6):635–663.
6. Oburoglu L, Tardito S, Fritz V, et al. Glucose and glutamine metabolism regulate human hematopoietic stem cell lineage specification. *Cell Stem Cell*. 2014;15(2):169–184.
7. Daud H, Browne S, Al-Majmaie R, Murphy W, Al-Rubeai M. Metabolic profiling of hematopoietic stem and progenitor cells during proliferation and differentiation into red blood cells. *N. Biotechnol.* 2016;33(1):179–186.
8. Chung J, Bauer DE, Ghamari A, et al. The mTORC1/4E-BP pathway coordinates hemoglobin production with L-leucine availability. *Sci. Signal.* 2015;8(372):ra34–ra34.
9. Bjursell G, Reichard P. Effects of thymidine on deoxyribonucleoside triphosphate pools and deoxyribonucleic acid synthesis in Chinese hamster ovary cells. *J. Biol. Chem.* 1973;248(11):3904–3909.
10. Larsson KM, Jordan A, Eliasson R, et al. Structural mechanism of allosteric substrate specificity regulation in a ribonucleotide reductase. *Nat. Struct. Mol. Biol.* 2004;11(11):1142–1149.
11. Melnyk S, Pogribna M, Miller BJ, et al. Uracil misincorporation, DNA strand breaks, and gene amplification are associated with tumorigenic cell transformation in folate deficient/repleted Chinese hamster ovary cells. *Cancer Lett.* 1999;146(1):35–44.
12. Hagen L, Peña-Diaz J, Kavli B, et al. Genomic uracil and human disease. *Exp. Cell Res.* 2006;312(14):2666–2672.
13. Toy G, Austin WR, Liao HI, et al. Requirement for deoxycytidine kinase in T and B

lymphocyte development. *Proc. Natl. Acad. Sci. U. S. A.* 2010;107(12):5551–5556.

14. Austin WR, Armijo AL, Campbell DO, et al. Nucleoside salvage pathway kinases regulate hematopoiesis by linking nucleotide metabolism with replication stress. *J. Exp. Med.* 2012;209(12):2215–2228.

15. Rossi GB, Migliaccio AR, Migliaccio G, et al. In vitro interactions of PGE and cAMP with murine and human erythroid precursors. *Blood*. 1980;56(1):74–9.

16. Pelus LM, Gentile PS. In vivo modulation of myelopoiesis by prostaglandin E2. III. Induction of suppressor cells in marrow and spleen capable of mediating inhibition of CFU-GM proliferation. *Blood*. 1988;71(6):1633–40.

17. Belegu M, Beckman B, Fisher JW. beta-Adrenergic blockade of prostaglandin E2- and D2-induced erythroid colony formation. *Am. J. Physiol. Physiol.* 1983;245(5):C322–C327.

18. Fisher JW, Radtke HW, Jubiz W, Nelson PK, Burdowski A. Prostaglandins activation of erythropoietin production and erythroid progenitor cells. *Exp. Hematol.* 1980;8 Suppl 8:65–89.

19. Di Pietro R, Di Giacomo V, Caravatta L, et al. Cyclic nucleotide Response Element Binding (CREB) protein activation is involved in K562 erythroleukemia cells differentiation. *J. Cell. Biochem.* 2007;100(4):1070–1079.

20. Wang J-M, Chao J-R, Chen W, et al. The Antiapoptotic Gene mcl-1 Is Up-Regulated by the Phosphatidylinositol 3-Kinase/Akt Signaling Pathway through a Transcription Factor Complex Containing CREB . *Mol. Cell. Biol.* 1999;19(9):6195–6206.

21. Kasper LH, Boussouar F, Ney PA, et al. A transcription-factor-binding surface of coactivator p300 is required for haematopoiesis. *Nature*. 2002;419(6908):738–743.

22. Oike Y, Takakura N, Hata A, et al. Mice homozygous for a truncated form of CREB-binding protein exhibit defects in hematopoiesis and vasculo-angiogenesis. *Blood*.

1999;93(9):2771–2779.

23. Boer AK, Drayer AL, Vellenga E. cAMP/PKA-mediated regulation of erythropoiesis. *Leuk. Lymphoma*. 2003;44(11):1893–1901.

24. Ikuta T, Sellak H, Odo N, Adekile AD, Gaensler KML. Nitric oxide-cGMP signaling stimulates erythropoiesis through multiple lineage-specific transcription factors: Clinical implications and a novel target for erythropoiesis. *PLoS One*. 2016;11(1):1–19.

25. Zhang W, Kadam S, Emerson BM, Bieker JJ. Site-Specific Acetylation by p300 or CREB Binding Protein Regulates Erythroid Kruppel-Like Factor Transcriptional Activity via Its Interaction with the SWI-SNF Complex. *Mol. Cell. Biol.* 2001;21(7):2413–2422.

26. Hsu CL, Lin W, Seshasayee D, et al. Equilibrative nucleoside transporter 3 deficiency perturbs lysosome function and macrophage homeostasis. *Science (80-.).* 2012;335(6064):89–92.

27. Baldwin SA, Yao SYM, Hyde RJ, et al. Functional characterization of novel human and mouse equilibrative nucleoside transporters (hENT3 and mENT3) located in intracellular membranes. *J. Biol. Chem.* 2005;280(16):15880–15887.

28. Govindarajan R, Leung GPH, Zhou M, et al. Facilitated mitochondrial import of antiviral and anticancer nucleoside drugs by human equilibrative nucleoside transporter-3. *Am. J. Physiol. - Gastrointest. Liver Physiol.* 2009;296(4):.

29. Priya TP, Philip N, Molho-Pessach V, et al. H syndrome: Novel and recurrent mutations in SLC29A3. *Br. J. Dermatol.* 2010;162(5):1132–1134.

30. Ramot Y, Sayama K, Sheffer R, et al. Early-onset sensorineural hearing loss is a prominent feature of H syndrome. *Int. J. Pediatr. Otorhinolaryngol.* 2010;74(7):825–827.

31. Campeau PM, Lu JT, Sule G, et al. Whole-exome sequencing identifies mutations in the

nucleoside transporter gene SLC29A3 in dysosteosclerosis, a form of osteopetrosis. *Hum. Mol. Genet.* 2012;21(22):4904–4909.

32. Elbarbary NS, Tjora E, Molnes J, et al. An Egyptian family with H syndrome due to a novel mutation in SLC29A3 illustrating overlapping features with pigmented hypertrichotic dermatosis with insulin-dependent diabetes and Faisalabad histiocytosis. *Pediatr. Diabetes*. 2013;14(6):466–472.

33. Nair S, Strohecker AM, Persaud AK, et al. Adult stem cell deficits drive Slc29a3 disorders in mice. *Nat. Commun.* 2019;10(1):.

34. An X, Schulz VP, Li J, et al. Global transcriptome analyses of human and murine terminal erythroid differentiation. *Blood*. 2014;123(22):3466–77.

35. Gautier E, Ducamp S, Leduc M, et al. Comprehensive Proteomic Analysis of Human Resource Comprehensive Proteomic Analysis of Human Erythropoiesis. *Cell Rep.* 2016;16(5):1470–1484.

36. Jackson EK, Mi Z, Dubey RK. The extracellular cAMP-adenosine pathway significantly contributes to the in vivo production of adenosine. *J. Pharmacol. Exp. Ther.* 2007;320(1):117–23.

37. Jackson EK, Raghvendra DK. The extracellular cyclic AMP-adenosine pathway in renal physiology. *Annu. Rev. Physiol.* 2004;66:571–99.

38. Daniels G, Ballif BA, Helias V, et al. Lack of the nucleoside transporter ENT1 results in the Augustine-null blood type and ectopic mineralization. *Blood*. 2015;125(23):3651–3654.

39. Chasis JA, Mohandas N. Erythrocyte membrane deformability and stability: Two distinct membrane properties that are independently regulated by skeletal protein associations. *J. Cell Biol.* 1986;

40. Warraich S, Bone DBJ, Quinonez D, et al. Loss of equilibrative nucleoside transporter 1

in mice leads to progressive ectopic mineralization of spinal tissues resembling diffuse idiopathic skeletal hyperostosis in humans. *J. Bone Miner. Res.* 2013;28(5):1135–1149.

41. Argyrousi EK, Heckman PRA, Prickaerts J. Role of cyclic nucleotides and their downstream signaling cascades in memory function: Being at the right time at the right spot. *Neurosci. Biobehav. Rev.* 2020;113:12–38.

42. Gauthier E, Guo X, Mohandas N, An X. Phosphorylation-dependent perturbations of the 4.1R-associated multiprotein complex of the erythrocyte membrane. *Biochemistry*. 2011;50(21):4561–4567.

43. Azouzi S, Collec E, Mohandas N, et al. The human Kell blood group binds the erythroid 4.1R protein: new insights into the 4.1R-dependent red cell membrane complex. *Br. J. Haematol.* 2015;171(5):862–871.

44. Tang, Tang. Erratum: The 30-kD domain of protein 4.1 mediates its binding to the carboxyl terminus of plCln, a protein involved in cellular volume regulation (Blood (1998) 92:4 (1442-1447)). *Blood*. 1999;93(3):1126.

45. Song A, Zhang Y, Han L, et al. Erythrocytes retain hypoxic adenosine response for faster acclimatization upon re-ascent. *Nat. Commun.* 2017;8:.

46. Lai Y, Tse C-M, Unadkat JD. Mitochondrial Expression of the Human Equilibrative Nucleoside Transporter 1 (hENT1) Results in Enhanced Mitochondrial Toxicity of Antiviral Drugs. *J. Biol. Chem.* 2004;279(6):4490–4497.

47. Lee EW, Lai Y, Zhang H, Unadkat JD. Identification of the mitochondrial targeting signal of the human equilibrative nucleoside transporter 1 (hENT1): Implications for interspecies differences in mitochondrial toxicity of fialuridine. *J. Biol. Chem.* 2006;281(24):16700–16706.

48. González-Vioque E, Torres-Torronteras J, Andreu AL, Martí R. Limited dCTP availability accounts for mitochondrial DNA depletion in mitochondrial

neurogastrointestinal encephalomyopathy (MNGIE). *PLoS Genet.* 2011;7(3):.

49. Azouzi S, Mikdar M, Hermand P, et al. Lack of the multidrug transporter MRP4/ABCC4 defines the PEL-negative blood group and impairs platelet aggregation. *Blood*. 2020;135(6):441–448.

50. Wu AG, Michejda M, Mazumder A, et al. Analysis and Characterization of Hematopoietic Progenitor Cells from Fetal Bone Marrow, Adult Bone Marrow, Peripheral Blood, and Cord Blood. *Pediatr. Res.* 1999;46(2):163–169.

51. Doulatov S, Notta F, Eppert K, et al. Revised map of the human progenitor hierarchy shows the origin of macrophages and dendritic cells in early lymphoid development. *Nat. Immunol.* 2010;11(7):585–593.

52. Mori Y, Chen JY, Pluvinage J V., Seita J, Weissman IL. Prospective isolation of human erythroid lineage-committed progenitors. *Proc. Natl. Acad. Sci. U. S. A.* 2015;112(31):9638–9643.

53. Paulson RF, Shi L, Wu DC. Stress erythropoiesis: New signals and new stress progenitor cells. *Curr. Opin. Hematol.* 2011;18(3):139–145.

54. Rose JB, Naydenova Z, Bang A, et al. Absence of equilibrative nucleoside transporter 1 in ENT1 knockout mice leads to altered nucleoside levels following hypoxic challenge. *Life Sci.* 2011;89(17–18):621–630.

55. Mendes-Silverio CB, Lescano CH, Zaminelli T, et al. Activation of soluble guanylyl cyclase with inhibition of multidrug resistance protein inhibitor-4 (MRP4) as a new antiplatelet therapy. *Biochem. Pharmacol.* 2018;152:165–173.

56. Cohen CM, Gascard P. Regulation and post-translational modification of erythrocyte membrane and membrane-skeletal proteins. *Semin. Hematol.* 1992;29(4):244–92.

57. Smith AS, Nowak RB, Zhou S, et al. Myosin IIA interacts with the spectrin-actin membrane skeleton to control red blood cell membrane curvature and deformability.

Proc. Natl. Acad. Sci. U. S. A. 2018;115(19):E4377–E4385.

58. Sanchez-Olea R, Emma F, Coghlan M, Strange K. Characterization of pI(Cln) phosphorylation state and a pI(Cln)-associated protein kinase. *Biochim. Biophys. Acta - Gen. Subj.* 1998;1381(1):49–60.

59. Meyer K, Korbmacher C. Cell swelling activates ATP-dependent voltage-gated chloride channels in M-1 mouse cortical collecting duct cells. *J. Gen. Physiol.* 1996;108(3):177–193.

60. Mayr BM, Canettieri G, Montminy MR. Distinct effects of cAMP and mitogenic signals on CREB-binding protein recruitment impart specificity to target gene activation via CREB. *Proc. Natl. Acad. Sci. U. S. A.* 2001;98(19):10936–10941.

61. Shaywitz AJ, Greenberg ME. CREB: A Stimulus-Induced Transcription Factor Activated by A Diverse Array of Extracellular Signals. *Annu. Rev. Biochem.* 1999;68(1):821–861.

62. Johannessen M, Delghandi MP, Moens U. What turns CREB on? *Cell. Signal.* 2004;16(11):1211–1227.

63. Sayama S, Song A, Brown BC, et al. Maternal erythrocyte ENT1–mediated AMPK activation counteracts placental hypoxia and supports fetal growth. *JCI Insight*. 2020;5(10):.

64. Suda T, Takubo K, Semenza GL. Metabolic regulation of hematopoietic stem cells in the hypoxic niche. *Cell Stem Cell*. 2011;9(4):298–310.

65. Simko V, Iuliano F, Sevcikova A, et al. Hypoxia induces cancer-associated cAMP/PKA signalling through HIF-mediated transcriptional control of adenylyl cyclases VI and VII. *Sci. Rep.* 2017;7(1):10121.

66. Xie Y, Shi X, Sheng K, et al. PI3K/Akt signaling transduction pathway, erythropoiesis and glycolysis in hypoxia (Review). *Mol. Med. Rep.* 2019;19(2):783–791.

67. Zwifelhofer NM, Cai X, Liao R, et al. GATA factor-regulated solute carrier ensemble reveals a nucleoside transporter-dependent differentiation mechanism. *PLOS Genet.* 2020;16(12):e1009286.

68. Kips JC, Joos GF, De Lepeleire I, et al. MK-571, a potent antagonist of leukotriene D4-induced bronchoconstriction in the human. *Am. Rev. Respir. Dis.* 1991;144(3 I):617–621.

69. Young RN. Development of novel leukotriene--based anti-asthma drugs: MK-886 and MK-571. *Agents Actions. Suppl.* 1991;34:179-87.

70. Gaddy JN, Margolskee DJ, Bush RK, Williams VC, Busse WW. Bronchodilation with a potent and selective leukotriene D4 (LTD4) receptor antagonist (MK-571) in patients with asthma. *Am. Rev. Respir. Dis.* 1992;146(2):358–363.

71. Hara Y, Sassi Y, Guibert C, et al. Inhibition of MRP4 prevents and reverses pulmonary hypertension in mice. *J. Clin. Invest.* 2011;121(7):2888–2897.

72. Lien LM, Chen ZC, Chung CL, et al. Multidrug resistance protein 4 (MRP4/ABCC4) regulates thrombus formation in vitro and in vivo. *Eur. J. Pharmacol.* 2014;737:159–167.

73. Cheepala SB, Pitre A, Fukuda Y, et al. The ABCC4 membrane transporter modulates platelet aggregation. *Blood*. 2015;126(20):2307–2319.

Figure legends

Figure 1. Red cell alterations in ENT1$_{null}$ individuals. (A) Western blot analysis of ENT1 expression in ENT1$_{null}$ RBC membranes from the three siblings. β-actin was used as loading control. **(B)** Blood smears of ENT1$_{null}$ individuals showing a macrocytosis and marked anisopoikilocytosis, characterized by the presence of RBCs with abnormal sizes and morphologies, including elliptocytes (black arrow), dacrocytes (red arrow) and schizocytes (blue arrow). Bar represents 10 μm. **(C)** Quantification of the different RBC populations was calculated from 300 RBCs per slide. **(D)** RBC deformability was assessed by an ektacytometry approach and elongation index relative to shear stress is shown for controls, P1, P2 and P3 and seven controls. **(E)** Osmoscan test of ENT1$_{null}$ RBCs from the three patients and a healthy control was monitored by ektacytometry. **(F)** The phosphoproteome of ENT1$_{null}$ (n=3) and control (n=5) RBC membranes was evaluated. Each dot represents a phosphorylated protein with blue dots corresponding to significantly hypo-phosphorylated (left) and hyper-phosphorylated (right) proteins. **(G)** Nucleotide-targeted metabolomic analysis of ENT1$_{null}$ (n=3; P1, blue; P2, green; P3, red triangles) and control (n=3; black circles) RBCs were performed and intracellular levels of deoxynucleotides and cyclic nucleotides (cAMP, cGMP) are shown**. (H)** Schematic representation of the variant filter strategy used to analyze the exome sequencing of ENT1$_{null}$ patients. Common mutations between P1 and P2, but absent in P3 (blue filled area) were filtered, candidate genes identified and their chromosomes are shown in the table. **(I)** Sanger sequencing confirmation of the c.559 G>T; p.Gly187Trp mutation on the *ABCC4* gene, showing the absence of the mutation in P3, and its presence in the heterozygous state in P1 and P2.

Figure 2. *Ex vivo* erythroid differentiation of CD34^{+} from ENT1$_{null}$ patients. (A) Erythroid differentiation of CD34^{+} progenitors was evaluated following rEPO-induced differentiation as

a function of expression of the erythroid surface markers GPA and Band3. Representative histograms showing the differentiation of $CD34^+$ progenitors from P1 (blue), P2 (green), P3 (red), controls (black) and non-specific IgG staining (grey shaded) are presented at days 5 and 8 of differentiation. Crossed boxes are present when insufficient cells were available for analyses. **(B)** Enucleation of erythroblasts from P1 and P2 $ENT1_{null}$ patients and respective controls (Ctrl1 and Ctrl2) was monitored at day 12 of erythroid differentiation as a function of DRAQ5 staining. Representative FACS plots and the percentages of enucleated cells (DRAQ5-negative) are shown. **(C)** The percentages of GPA^+ cells and $Band3^+$ cells were quantified at day 5 of differentiation. Mean percentages ± SEM for controls (black dots, n=7 independent experiments) and P3 $ENT1_{null}$ patient progenitors (red triangles, n=2 independent experiments in duplicate) are presented. ****p<0.0001; ***p=0.0002 (unpaired t-test). **(D)** Growth curves of progenitors from the three $ENT1_{null}$ patients (P1, n=1; P2, n=1; P3, n=4) and healthy donors (n=9) were evaluated at indicated days of erythroid differentiation. **p<0.01 (unpaired t-test). **(E)** Representative images of May-Grünwald Giemsa–stained cytospins at day 5 of rEPO differentiation of control and P3 $ENT1_{null}$ progenitors are shown (upper panel). The bar represents 10 µm. Quantification of the different cell types is presented (n=3 independent experiments, lower panel). **(F)** Characterization of P3 and control progenitors were evaluated at day 7 of the expansion phase (before addition of rEPO) as a function of IL-3R, CD34, CD36, CD38 and CD33. Representative histograms showing non-specific IgG staining (grey shaded), control (black line) and P3 (red line) staining are presented. The expression of CD34 and CD36 surface markers was analyzed on the $IL\text{-}3R^{neg}$ cells, in order to identify BFU-E ($IL\text{-}3R^-CD34^+CD36^-$, green square) and CFU-E ($IL\text{-}3R^-CD34^-CD36^+$, red square) and representative percentages are indicated. **(G)** $CD34^+$ progenitor cells from a healthy donor and the P3 $ENT1_{null}$ patient were cultured in a methylcellulose semi-solid culture assay and representative images

of the generated colonies are shown. Quantification of the generated colonies is presented for two technical replicates.

Figure 3. shRNA-Mediated Knockdown of ENT1 negatively impacts *ex vivo* erythroid differentiation. (A) Schematic representation of the schema used for *ex vivo* human erythropoiesis and the experimental design. Cord blood $CD34^+$ cells were differentiated using a three-phase culture system (containing rEPO) that recapitulates human erythropoiesis up to the enucleated reticulocyte. Cells were transduced at day 4 of the expansion phase with a lentiviral vector harboring an ENT1 shRNA or scramble together with a GFP reporter gene. Representative MGG-stained cells from healthy control are shown for corresponding differentiation stages. **(B)** The evolution of surface ENT1 expression during rEPO-induced (3 U/ml) erythroid differentiation was monitored by flow cytometry and representative histograms showing non-specific IgG staining (grey shaded) and specific (black line) staining at days 0, 3, 7, and 10 of erythroid differentiation are presented, differentiating negatively and positively stained cells. The geometric mean fluorescence intensity (GMFI) is indicated in each histogram. GMFIs from 3 independent experiments were quantified and are presented as means ± SEM (right panel). **(C)** Progenitors transduced with shControl and shENT1 vector were FACS-sorted on the basis of GFP expression 3 days post transduction and ENT1 mRNA expression levels were analyzed by qRT-PCR and normalized to actin mRNA. mRNA±SD relative to control cells is presented (n=3; unpaired t-test; ****, $p<0.0001$). **(D)** Transduced progenitors were cultured in the presence or absence of rEPO as indicated. The evolution of shRNA-expressing cells was followed and the percentages of GFP^+ cells relative to day 1 are shown. Results correspond to data obtained from three independent experiments. **(E)** Progenitors transduced with the shControl and shENT1 vectors were FACS-sorted on the basis of GFP expression and then differentiated in the presence of EPO. Cells were counted at the indicated days and growth curves are presented for shENT1-GFP^+ (grey line) and shControl-GFP^+ (black line) cells. Data

presented are means ± SEM of four independent experiments; *p<0.05, ***p<0.001.**(F)** Progenitors were transduced with shControl or shENT1 vectors, both harboring a GFP transgene. Gene transfer efficiency was evaluated as a function of GFP expression 3 days following transduction and representative histograms are shown (top panels). The percentages of cells expressing GPA and CD71 were evaluated by flow cytometry and representative profiles in GFP^- and GFP^+ subsets are presented. The percentages of positively-stained cells are indicated. **(G)** Erythroid differentiation of control-GFP- and shENT1-GFP-transduced progenitors was monitored as a function of GPA and CD71 expression within the GFP^+ cells. The percentages of GPA^+ and $CD71^+$ cells ± SEM in control (black circles) and shENT1-GFP (grey triangles) transduced progenitors are shown at days 3, 5 and 7 of culture (n=3; Unpaired t-test; *p<0.05, **, p<0.01, ***p<0.001). **(H)** Enucleation was monitored at day 10 of differentiation as a function of Syto-16 staining and the percentages of Syto-16-negative cells are presented (n=3 independent experiments; unpaired t-test; *, p=0.02). **(I)** At day 4 of differentiation, cells were FACS-sorted on the basis of GFP expression and differentiation was continued until day 10. Erythroid differentiation was monitored as a function of Band3 expression and myeloid differentiation was monitored by CD11a/CD33 surface expression (black) and non-specific control IgG staining (grey). Representative histograms and quantification are shown within GFP^+ cells. (n=3 independent experiments; *p<0.05).

Figure 4. Genetic depletion of *Ent1* in mice hampers erythroid lineage commitment in the BM. (A) Increased size of RBCs in *Ent1*$^{-/-}$ mice as compared to WT mice. EDTA-anticoagulated mouse blood was used for Wright-Giemsa staining and representative blood smears are shown. **(B)** Schematic of MEP, CMP and GMP progenitors as well as the differentiation to mature red cells and granulocytes. The flow cytometry-based analytic strategy to identify the different populations is presented. **(C)** Representative FACS analysis of hematopoietic progenitor cells of BM of 8-12-week old *Ent1*$^{-/-}$ and WT mice. The number of

$Lin^{-}cKit^{+}$, CMP, MEP and GMP cells per 10^6 BM cells (excluded RBCs) are presented in WT and *Ent1*$^{-/-}$ mice (n=9, *p < 0.05). **(D)** Erythroid and myeloid cells were evaluated as a function of Ter119 and Gr-1 staining, respectively, and representative dot plots are shown (left panel). Quantification of the percentages of $Ter119^{+}$ cells versus $Gr\text{-}1^{+}$ cells in BM of *Ent1*$^{-/-}$ and WT mice are presented (right panel) as means ± SEM with each point corresponding to data from one mouse (*p < 0.05). **(E)** Quantification of spleen body weight ratio in *Ent1*$^{-/-}$ and WT mice (*p < 0.05). **(F)** Representative FACS analyses of differentiated erythroblasts by CD71 and Ter119 staining in spleens of *Ent1*$^{-/-}$ and WT mice (left). The developmental stage of erythroblasts was indicated by population I, II, III, and IV. The quantification of these populations is displayed in the right (*p < 0.05). **(G)** Representative FACS plots are shown for splenic $Ter119^{+}$ cells *versus* $Gr\text{-}1^{+}$ cells in *Ent1*$^{-/-}$ and WT mice (left) and quantification of data in individual mice are presented as means ± SEM (right; *p < 0.05). **(H)** Biotin-labeled RBCs in WT (black circles) and *Ent1*$^{-/-}$ (red squares) are shown as a function of time post biotin labelling. Means ± SEM of 5 mice in each group are shown.

Figure 5. ENT1-mediated adenosine uptake induced cyclic nucleotide accumulation and enhanced *in vitro* erythropoiesis. (A) $CD34^{+}$ progenitors from peripheral blood of healthy donors were stimulated with rEPO in the absence or presence of adenosine (15 μM) at day 0 of the differentiation phase. Terminal differentiation was monitored as a function of the α4-integrin/ Band3 profiles of GPA^{pos} cells. Differentiation steps can be followed as α4-$integrin^{high}$/$Band3^{low}$ (Quadrant 1, Q1), α4-$integrin^{med}$/$Band3^{med}$ (Q2), and α4-$integrin^{low}$/$Band3^{high}$ (Q3). Expression levels of α4-integrin and Band3 levels inside GPA^{+} cells are shown at day 5, 9 and 12 for control and adenosine-treated cells. **(B)** The percentages of α4-$integrin^{high}$/$Band3^{low}$, α4-$integrin^{med}$/$Band3^{med}$, and α4-$integrin^{low}$/$Band3^{high}$ in control (black circles) and adenosine-treated (red triangles) cells are plotted in histograms. Results are expressed as the mean cell % ± SEM. Multiple comparisons of two-way Anova statistical test

were performed and corresponding significant differences are shown. *p<0.05; **p<0.005; ***p<0.001. **(C)** Representative images of May-Grünwald Giemsa–stained cytospins of control and adenosine-treated cells (+ADO) at day 7 of differentiation. Bar represents 10 µm. **(D)** Surface expression levels of GPA and Band3 erythroid markers and CD11a and CD33 myeloid markers were evaluated by flow cytometry at day 7 of rEPO-induced erythroid differentiation. Representative histograms showing GFP^{pos} gated cells for shControl (filled black histograms), shENT1 (empty black histograms) and shENT1 treated with adenosine (empty red histograms) transduced cells are shown (left panel); grey shaded histograms correspond to non-specific IgG staining and were used to evaluate positive staining. Quantification of three independent experiments is presented for each marker (right panel). Ns, non significant, *p<0.05, **p<0.01, ***p<0.001, ****p<0.0001. **(E)** shENT1-and shcontrol transduced $CD34^{+}$ cells were stimulated with EPO and cultured in absence or presence of adenosine (15 µM). Surface expression levels of GPA were monitored at indicated days and plotted in scatter dot plot histograms as mean cell % ± SEM. Two-way Anova statistical test was performed and statistical significance is indicated (n=3 independent experiments). **p<0.01; ***p<0.001; ****p<0.0001. **(F)** Intracellular concentrations of cAMP, cGMP and adenine nucleotides inside erythroid precursors at day 3 of erythroid differentiation were measured by a liquid chromatography–mass spectrometry approach, and representative bar histograms are shown for control (black) and adenosine-treated cells (red). Results are expressed as mean ± SEM n=3. *p<0.05; **p<0.01; ***p<0.001 (paired t-test). (G) The phosphorylation state of CREB (Ser133) was evaluated by intracellular staining using an anti-phosphoCREB antibody and analyzed by flow cytometry throughout erythroid terminal differentiation. GMFI (left panel) and percentages of $P\text{-}CREB^{+}$ cells (right panel) are presented at the indicated days as means ± SEM of four independent experiments. **p<0.01, ***p<0.001. **(H)** Phosphorylation of PKA RIIβ (Ser114) was monitored at the indicated time points. GMFI (left panel) and the percentages

of P-PKA$^+$ cells (right panel) are shown as means ± SEM of four independent experiments. *p<0.05, **p<0.01.

Figure 6. Reduced ABCC4 activity enhances *in vitro* erythropoiesis of human CD34$^+$ cells as well as erythropoiesis in WT and *Ent1*$^{-/-}$ mice and enhances. (A) CD34$^+$ cells from healthy donors were cultured in the presence or absence of MK-571 (100 μM), initiated 24 hours after CD34$^+$ selection. GPA expression was monitored at day 3 of rEPO-induced erythroid differentiation and representative FACS histograms of control (black histogram) and MK571-treated progenitors (orange histogram) are presented, including percentages of GPA$^+$ cells and GFMI (left panels). Shaded grey histograms correspond to unstained negative controls specifying negative gating. GMFI (middle panel) and the percentages of GPA$^+$ cells (right panel) were quantified and means ± SEM of three independent experiments are shown. *p<0.05. (B) Erythroblast maturation was monitored at day 12 of differentiation in the presence or absence of MK-571 by α4-integrin/Band3 profiles of GPA^{pos} cells. Representative dot plots are shown (left panel), and the percentages of cells in each quadrant are indicated. Quantification of cells in the more immature α4-integrin^{high}/Band3^{low} and α4-integrin^{med}/Band3^{med} subsets as compared to the more mature α4-integrin^{low}/Band3^{high} subset is presented for 3 independent experiments (right panel). *p<0.05. **(C)** Erythroblast enucleation was evaluated as a function of Syto16 nucleic acid staining and representative dot plots indicating the percentages of Syto16- enucleated cells (left) and quantification of enucleated cells in 3 independent experiments are presented (right). *p<0.05. **(D)** Hematological parameters of wild-type and *Ent1*$^{-/-}$ mice under control conditions or following a 6-day treatment with MK-571**.** *p <0.05, **p <0.01, ***p <0.001, wild type treated *versus* wild type, *Ent1*$^{-/-}$ treated versus *Ent1*$^{-/-}$ untreated. **(E)** Quantification of CMP, MEP and GMP in BM of WT and *Ent1*$^{-/-}$ mice in the absence or presence of MK-571 treatment (10 mg/kg q.o.d. for one week, n=4-6). **(F)** Frequency of Lin$^-$c-kit$^+$ cells in BM and spleen of WT and Ent1$^{-/-}$ mice treated

or not with MK-571. **(G)** Quantification of the frequencies of $Ter119^+$ and $Gr\text{-}1^+$ cells in BM of untreated and MK-571-treated WT and *Ent1*$^{-/-}$ mice are presented (n=4-6). ns, non significant, *p < 0.05, **p < 0.01.

Figure 6

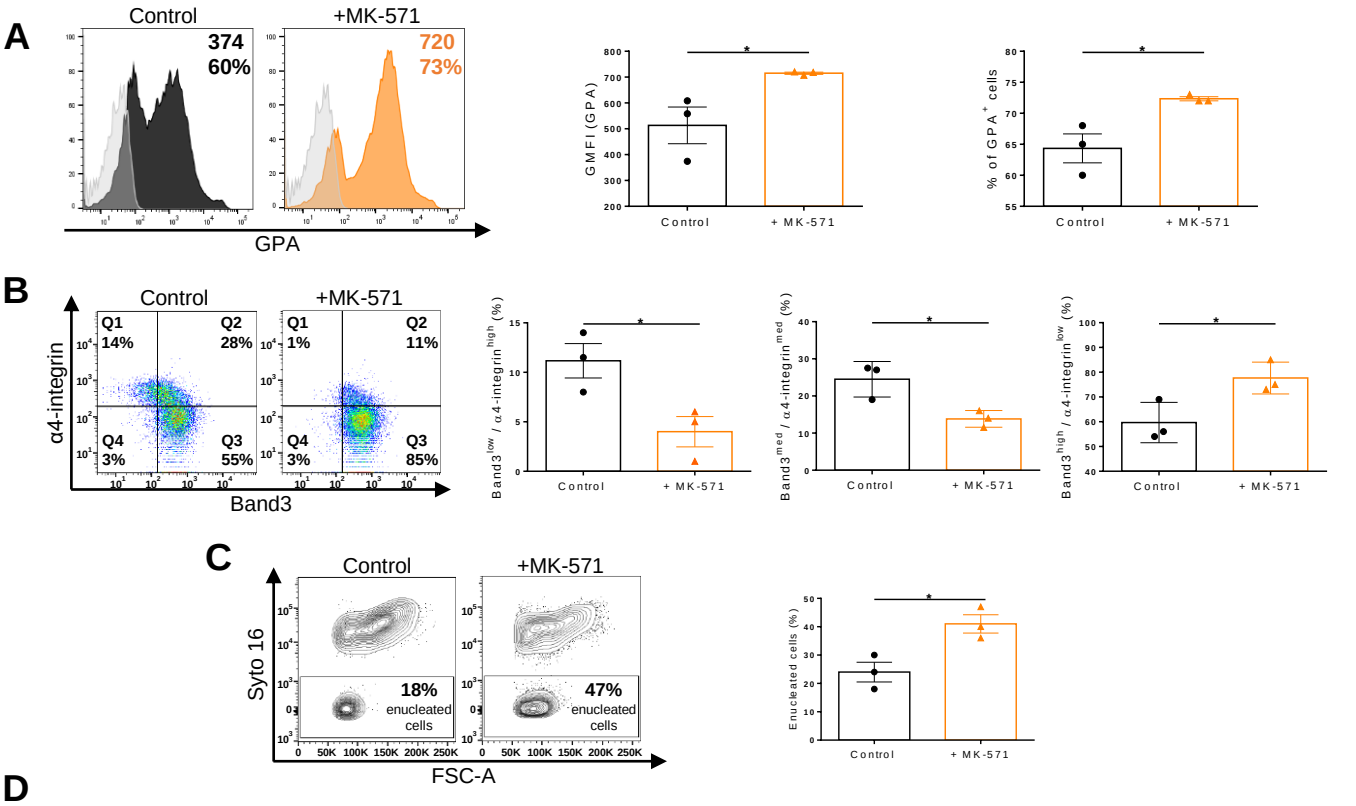

D

	Wild type (untreated, n=6)	Wild type (+MK-571, n=4)	Ent1$^{-/-}$ (untreated, n=6)	Ent1$^{-/-}$ (+MK-571, n=4)
RBC ($1x10^6$cells μl^{-1})	9.19 ± 0.16	9.78 ± 0.30*	7.22 ± 0.61***	8.31 ± 0.31*
Hb (g dl^{-1})	13.26 ± 0.15	13.75 ± 0.31*	12.25 ± 0.43*	13.70 ± 0.54**
HCT (%)	43.11 ± 1.11	45.25 ± 0.86*	39.41 ± 2.08*	45.10 ± 2.05**
MCV (fl)	49.03 ± 2.02	46.2 ± 0.64*	56.98 ± 2.52**	55.95 ± 0.91
MCH (pg)	15.03 ± 0.63	14.65 ± 0.13	17.21 ± 0.92**	16.8 ± 0.20
Retic (%)	3.23 ± 0.18	4.51 ± 0.23*	4.81 ± 0.26	5.80 ± 0.46*
WBC ($1x10^3$cells μl^{-1})	6.60 ± 1.96	2.69 ± 1.85	3.31 ± 2.27	3.01 ± 1.25

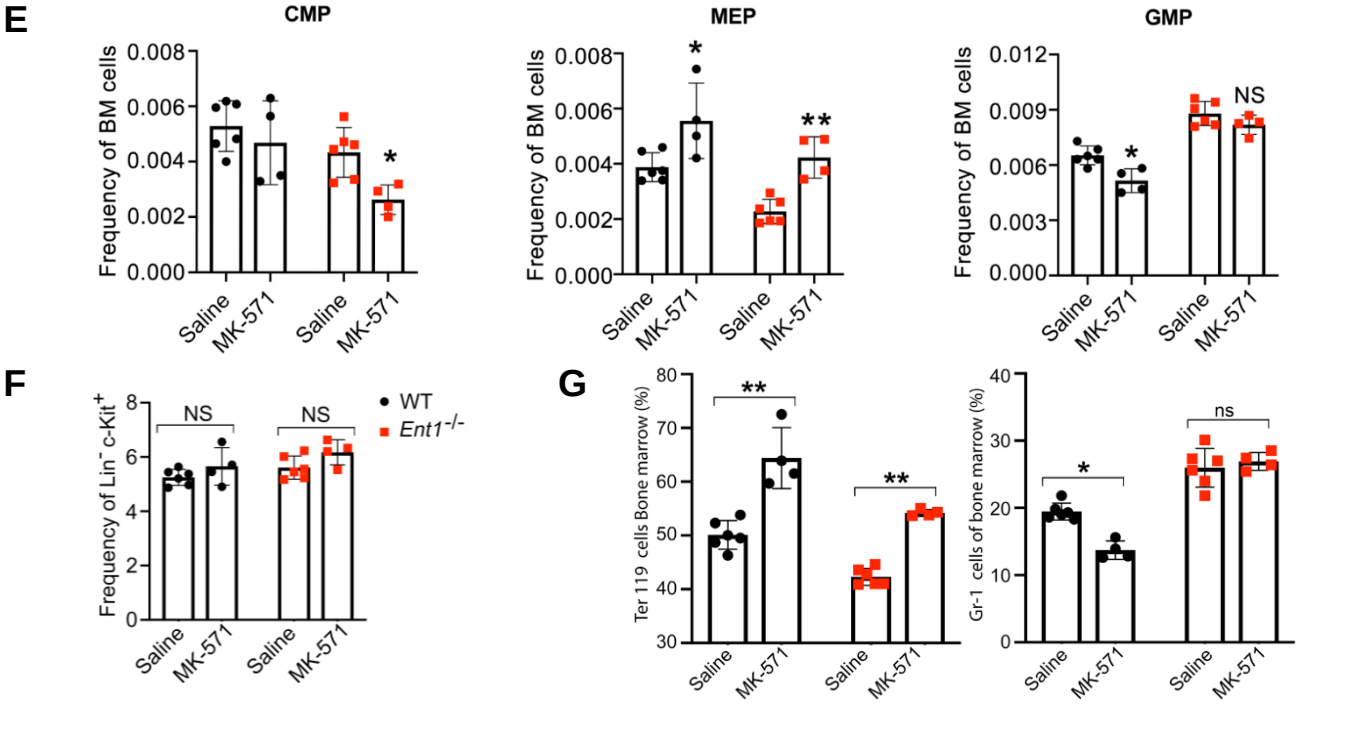

Figure 5

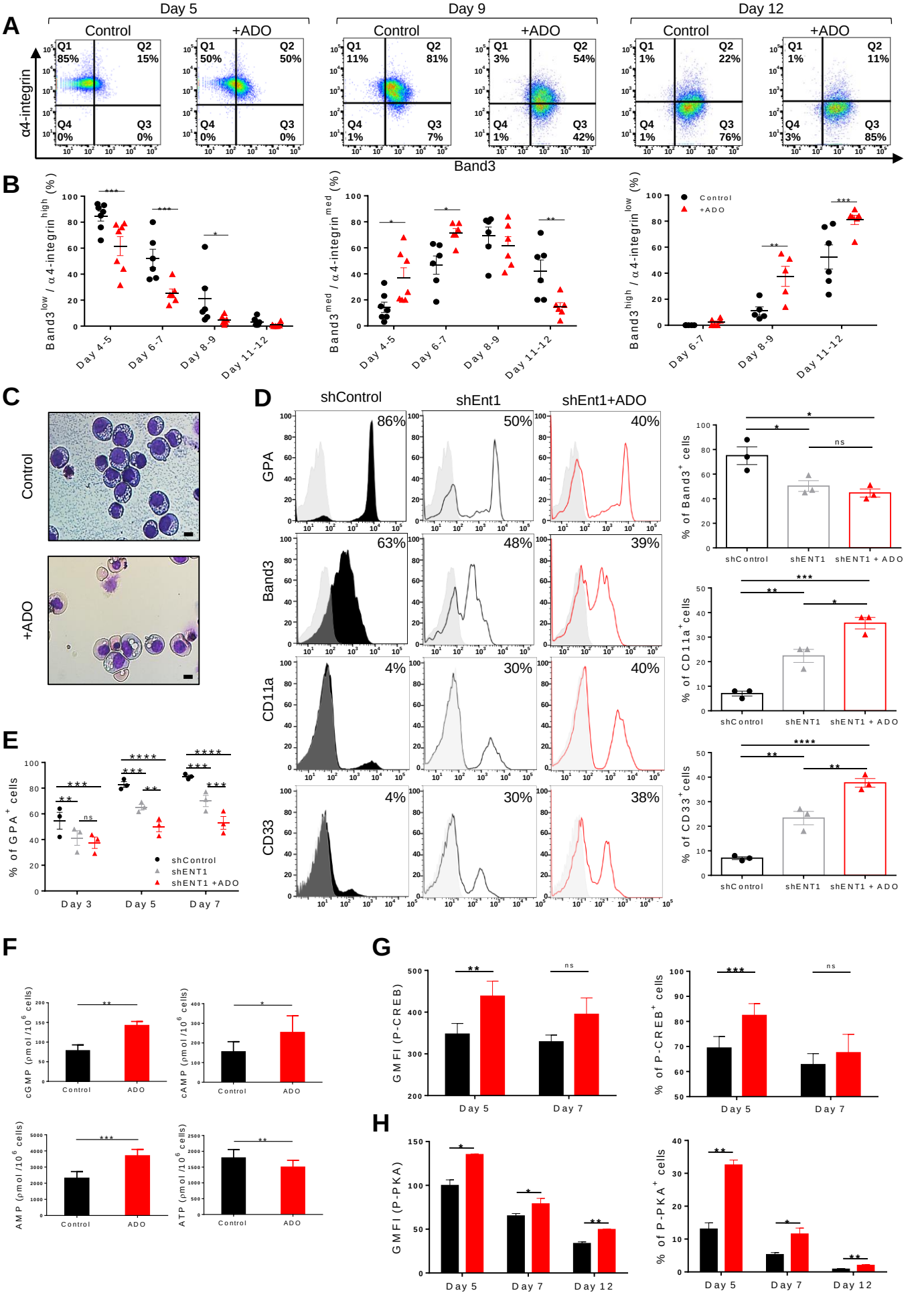
A
Day 5
Day 9
Day 12
Control
+ADO
α4-integrin
Band3
Q1 85%
Q2 15%
Q4 0%
Q3 0%
Q1 50%
Q2 50%
Q4 0%
Q3 0%
Q1 11%
Q2 81%
Q4 1%
Q3 7%
Q1 3%
Q2 54%
Q4 1%
Q3 42%
Q1 1%
Q2 22%
Q4 1%
Q3 76%
Q1 1%
Q2 11%
Q4 3%
Q3 85%
B
Band3low / α4-integrinhigh (%)
Band3med / α4-integrinmed (%)
Band3high / α4-integrinlow (%)
Day 4-5
Day 6-7
Day 8-9
Day 11-12
Control
+ADO
C
Control
+ADO
D
shControl
shEnt1
shEnt1+ADO
GPA
Band3
CD11a
CD33
86%
50%
40%
63%
48%
39%
4%
30%
40%
4%
30%
38%
% of Band3+ cells
% of CD11a+ cells
% of CD33+ cells
shControl
shENT1
shENT1 + ADO
E
% of GPA+ cells
Day 3
Day 5
Day 7
shControl
shENT1
shENT1 +ADO
F
cGMP (pmol /10^6 cells)
cAMP (pmol /10^6 cells)
AMP (pmol /10^6 cells)
ATP (pmol /10^6 cells)
Control
ADO
G
GMFI (P-CREB)
% of P-CREB+ cells
Day 5
Day 7
H
GMFI (P-PKA)
% of P-PKA+ cells
Day 5
Day 7
Day 12

Figure 4

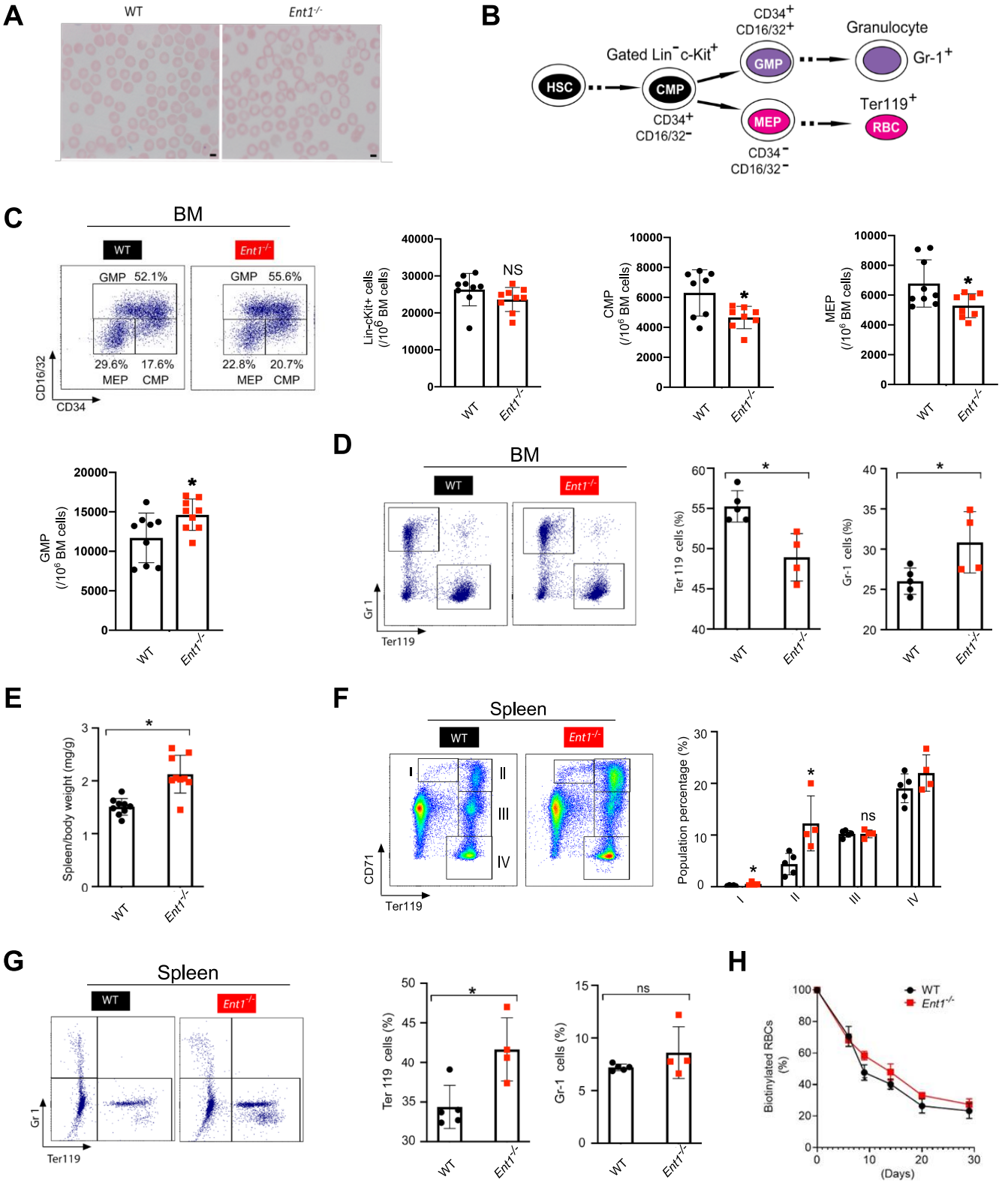
A
WT
Ent1-/-
B
HSC
CMP
GMP
MEP
RBC
Gated Lin-c-Kit+
CD34+ CD16/32+
CD34+ CD16/32-
CD34- CD16/32-
Granulocyte
Gr-1+
Ter119+
C
BM
WT
Ent1-/-
GMP 52.1%
GMP 55.6%
29.6% MEP
17.6% CMP
22.8% MEP
20.7% CMP
CD16/32
CD34
Lin-cKit+ cells (/10^6 BM cells)
NS
CMP (/10^6 BM cells)
MEP (/10^6 BM cells)
GMP (/10^6 BM cells)
D
BM
Gr 1
Ter119
Ter 119 cells (%)
Gr-1 cells (%)
E
Spleen/body weight (mg/g)
F
Spleen
CD71
Ter119
I
II
III
IV
Population percentage (%)
ns
G
Spleen
Gr 1
Ter119
Ter 119 cells (%)
Gr-1 cells (%)
H
Biotinylated RBCs (%)
(Days)

Figure 3

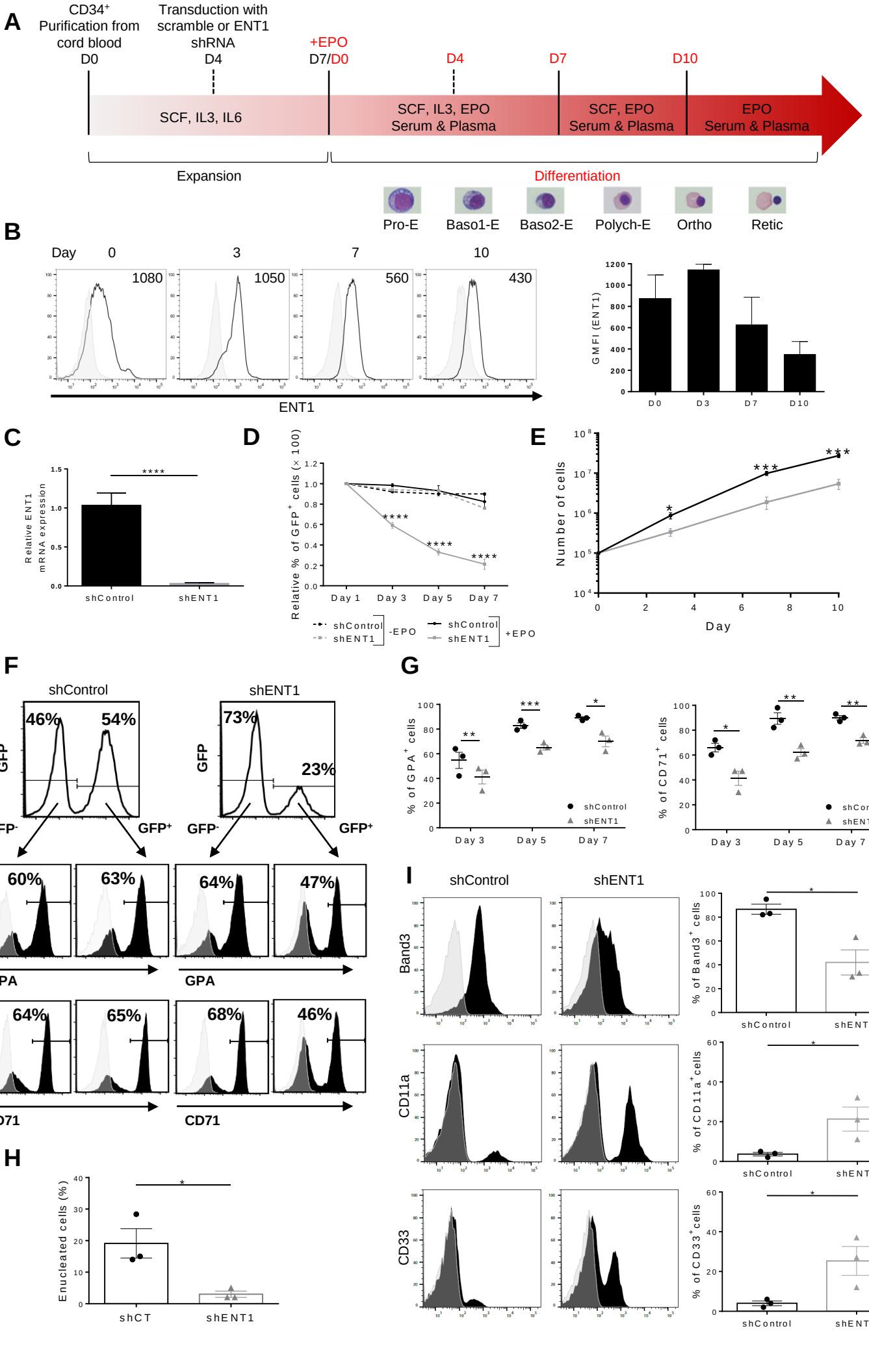
A
CD34+ Purification from cord blood D0
Transduction with scramble or ENT1 shRNA D4
+EPO D7/D0
D4
D7
D10
SCF, IL3, IL6
SCF, IL3, EPO Serum & Plasma
SCF, EPO Serum & Plasma
EPO Serum & Plasma
Expansion
Differentiation
Pro-E
Baso1-E
Baso2-E
Polych-E
Ortho
Retic
B
Day 0 3 7 10
1080
1050
560
430
ENT1
GMFI (ENT1)
D0 D3 D7 D10
C
Relative ENT1 mRNA expression
shControl
shENT1
D
Relative % of GFP+ cells (× 100)
Day 1 Day 3 Day 5 Day 7
shControl shENT1 -EPO
shControl shENT1 +EPO
E
Number of cells
Day
F
shControl
shENT1
46% 54%
73% 23%
GFP
GFP- GFP+
60% 63% 64% 47%
GPA
64% 65% 68% 46%
CD71
G
% of GPA+ cells
% of CD71+ cells
Day 3 Day 5 Day 7
shControl shENT1
H
Enucleated cells (%)
shCT shENT1
I
shControl shENT1
Band3
CD11a
CD33
% of Band3+ cells
% of CD11a+ cells
% of CD33+ cells

Figure 2

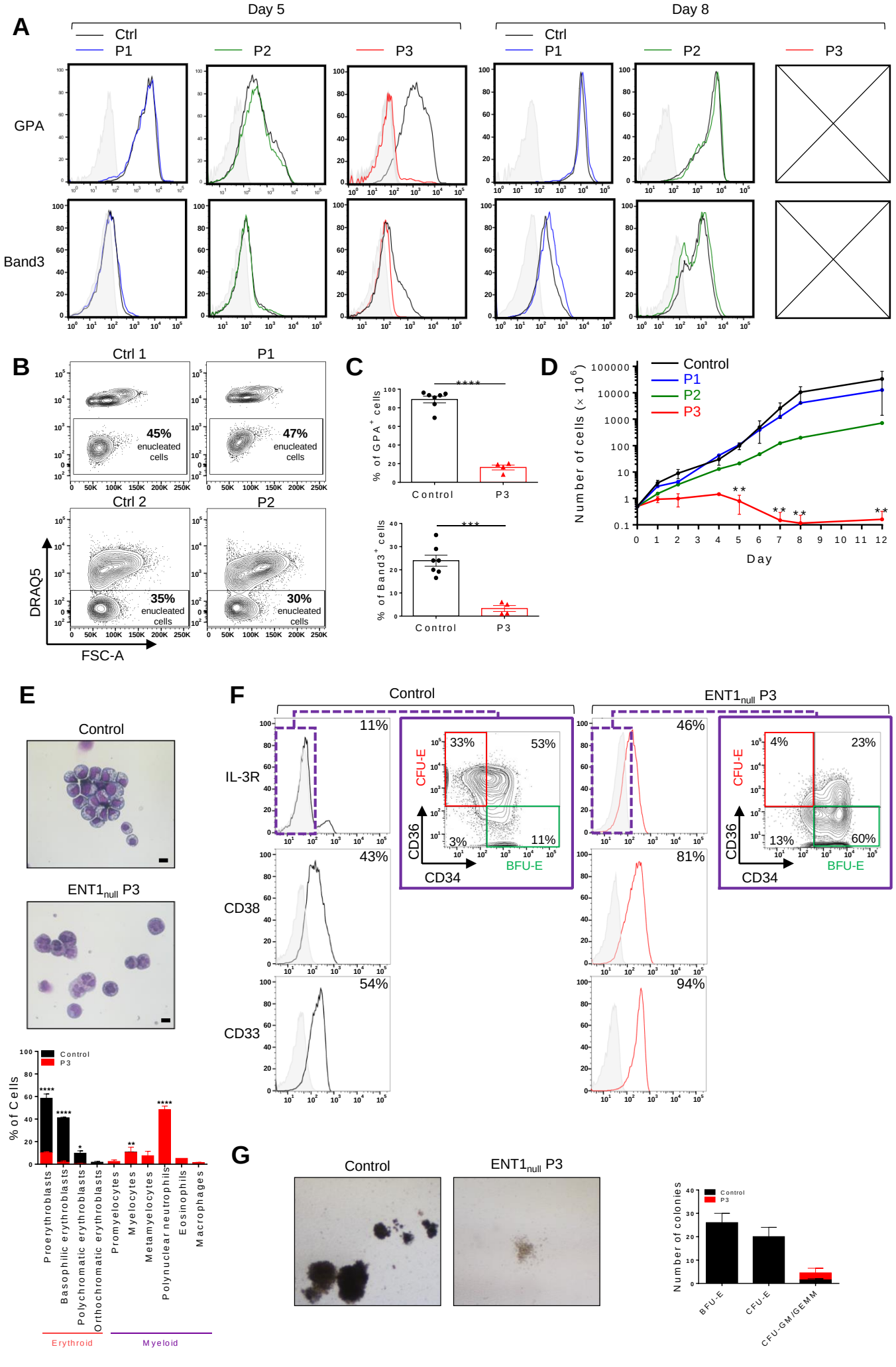
A
Day 5
Day 8
Ctrl
P1
P2
P3
GPA
Band3
B
Ctrl 1
P1
Ctrl 2
P2
45% enucleated cells
47% enucleated cells
35% enucleated cells
30% enucleated cells
DRAQ5
FSC-A
C
% of GPA+ cells
% of Band3+ cells
Control
P3
D
Control
P1
P2
P3
Number of cells (× 10^6)
Day
E
Control
ENT1null P3
% of Cells
Proerythroblasts
Basophilic erythroblasts
Polychromatic erythroblasts
Orthochromatic erythroblasts
Promyelocytes
Myelocytes
Metamyelocytes
Polynuclear neutrophils
Eosinophils
Macrophages
Erythroid
Myeloid
F
Control
ENT1null P3
IL-3R
CD38
CD33
CFU-E
BFU-E
CD36
CD34
11%
43%
54%
33%
53%
3%
11%
46%
81%
94%
4%
23%
13%
60%
G
Control
ENT1null P3
Number of colonies
BFU-E
CFU-E
CFU-GM/GEMM

Figure 1

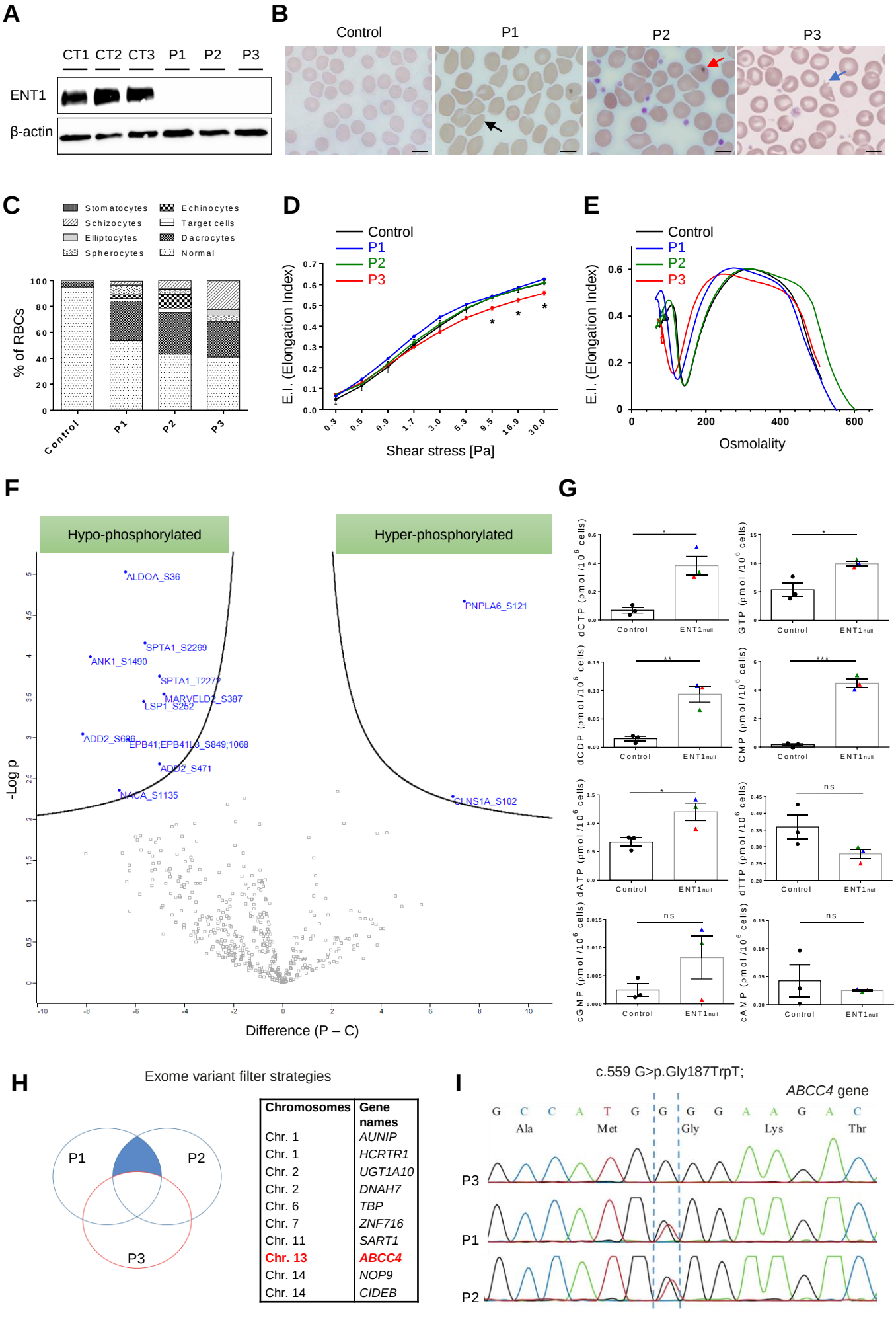

H

Exome variant filter strategies

Chromosomes	Gene names
Chr. 1	*AUNIP*
Chr. 1	*HCRTR1*
Chr. 2	*UGT1A10*
Chr. 2	*DNAH7*
Chr. 6	*TBP*
Chr. 7	*ZNF716*
Chr. 11	*SART1*
Chr. 13	***ABCC4***
Chr. 14	*NOP9*
Chr. 14	*CIDEB*

I